Supporting Information for

Suppressing the Universal Occurrence of Microscopic Liquid Residues on Super-Liquid-Repellent Surfaces

*Shilin Huang, Juan Li,† Liwei Chen, and Xuelin Tian**

State Key Laboratory of Optoelectronic Materials and Technologies, School of Materials Science and Engineering, Sun Yat-sen University, Guangzhou 510006, China

Key Laboratory for Polymeric Composite & Functional Materials of Ministry of Education, Sun Yat-sen University, Guangzhou 510006, China

* Corresponding Author. E-mail: tianxuelin@mail.sysu.edu.cn

† Present Addresses: School of Traditional Chinese Medicine Resources, Guangdong Pharmaceutical University, Guangzhou 510006, China

Contents

- Figure S8. No liquid residues observed when a mercury drop slides on micropillared surface.
- Figure S9. Simulation details of receding contact line on a micropillared surface.
- Figure S10. Formation of microscopic liquid residues on PFPE-coated SLR surfaces with different microstructures.

Supporting Tables

- Table S1. Contact angles, fitting parameters and governing dimensionless numbers for ionic liquid (N^+S^-) on the model SLR surfaces.
- Table S2. Physical properties of the test liquids and their contact angles on the model SLR surfaces.

Supporting Movies

- Movie S1. Stepwise pinning-depinning processes of the receding contact line on the micropillared SLR surfaces with different coatings.
- Movie S2. Evolution dynamics (time resolution: 10^{-4} s) of micro-capillary bridges on SLR surfaces with different coatings.
- Movie S3. High-speed evolution dynamics (time resolution: 10^{-5} s) of micro-capillary bridges on SLR surfaces with different coatings, showing the detailed necking and pinch-off processes occurring in the last 0.1 ms.

- Movie S4. High-speed evolution dynamics (time resolution: 10^{-5} s) of micro-capillary bridge for a metal liquid (Hg) drop on the micropillar, showing neither necking nor pinch-off of the micro-capillary bridge.

Experimental Section

Materials. 4-inch p-type silicon wafers with 1-μm-thick silicon dioxide (SiO_2) layers (Kaihua Shunchen Electronic Technology Co., Ltd.) were used to fabricate the micropillared surfaces. AZ-nLof 2035 photoresist (MicroChemicals, GmbH) was used for photolithography. *1H, 1H, 2H, 2H*-perfluorooctyltrichlorosilane (PFOS, 97%, Aldrich) and trimethoxysilyl-terminated perfluorinated polyether (PFPE, Optool, Daikin) were used for surface coating. The test liquids, polydimethysiloxane (PDMS, molecular weight = 6000 g/mol, Alfa), *n*-hexadecane (99%, Alfa), ionic liquid dimethylbis(*β*-hydroxyethyl) ammonium methanesulfonate ($C_6H_{16}O_2N^+CH_3SO^{3-}$, N^+S^-, Shanghai Chengjie Chemical Co. Ltd.), oleic acid (AR, Shanghai Macklin Biochemical Co., Ltd.), mercury (ACS, 99.9995% metals basis, Aladdin), and colloidal silica dispersion (Ludox SM, 7 nm), were

used without further purification. Sodium chloride (AR, 99.5%, Greagent) was dissolved in Milli-Q water to obtain salt solution with desired concentration. Rhodamine B (RG, Adamas beta, Shanghai, China) was used to fluorescently label the test liquids.

Fabrication of micropillared surfaces. The micropillared surfaces were fabricated on 4-inch *p*-type silicon wafers covered with 1-μm-thick SiO_2 films. First, the photoresist AZ-nLof 2035 was patterned on the wafers through photolithography (uPG501 mask writer, Heidelberg Instruments). The patterns were then transferred onto SiO_2 using reactive ion etching (Oxford Instruments, PlasmaPro System 100, pressure = 30 mTorr, power = 200 W, CHF_3 flow rate = 12 sccm, Ar flow rate = 38 sccm, etching time = 20 min). The T-shaped microstructure was introduced by two inductively coupled plasma (ICP) etching processes (Oxford Instruments, PlasmaPro System 100ICP180). For the first etching process, the operation conditions were: pressure = 6 mTorr, ICP generator power = 800 W, radio frequency (RF) generator power = 50 W, temperature = 10 °C, SF_6 flow rate = 30 sccm, O_2 flow rate = 15 sccm and etching time = 4 min. For the second etching process, the operation conditions were: pressure = 6 mTorr, ICP generator power = 500

W, RF generator power = 50 W, temperature = 25 °C, SF_6 flow rate = 30 sccm, O_2 flow rate = 10 sccm, and etching time = 2 min.

Surface coating. The microstructured surfaces and flat surfaces were treated with air plasma (Harrick Plasma, PDC-002, RF power = 30W) for 15 min to introduce hydroxyl groups. Afterwards, the surfaces were coated with PFOS by exposing them to PFOS vapor in a vacuumed desiccator at ambient temperature for 2 h. Vacuum (-0.095 MPa) was applied to the desiccator to promote evaporation of PFOS (20 μL). For complete coating of the surface, this silanization process was repeated for 3 times. For PFPE coating, the surfaces with hydroxyl groups were dipped into 0.4 wt% PFPE solution in Novec 7200 for about 10 s. Then the surfaces were carefully withdrawn from the solution and dried in air for 1 min (relative humility ~60% at 25 ^oC), followed by heating at 130 ^oC for 30 min. Finally, the samples were thoroughly cleaned using hexane, ethanol and water. The thicknesses of the PFOS and PFPE coatings were 1.7±0.1 nm and 3.6±0.2 nm, respectively, as measured by an ellipsometer (Alpha-SE, J.A. Woollam) using Cauchy model.

Surface characterization. Scanning electron microscope (SEM) images were obtained using a FIB-SEM system (Auriga, Zeiss) operated at a voltage of 5 kV. An atomic force microscope (Bruker Icon Dimension) was used to measure the surface roughness. X-ray photoelectron spectroscopy (XPS, ESCALAB 250, Thermo Fisher Scientific) was used to confirm the successful grafting of PFOS and PFPE on the surfaces. A goniometer (Krüss, DSA100S) was used to measure the contact angles. For measuring the sliding angle, a 5 μL liquid drop was first deposited on the sample surface before the sample was slowly tilted at 5°/min. The sliding angles was recorded when the drop started to slide on the surface. The advancing and receding angles were measured at the advancing front and receding tail of the sliding drop, respectively. At least three drops were used to determine the contact angles. The test liquids for contact angle measurements in this study include milli-Q water, hexadecane, and ionic liquid (N^+S^-).

Optical imaging. Leica DVM6 was used for observing the microstructures on the goose feather. Leica DM2700 M microscope was used for obtaining the other microscope images. Fluorescent images were obtained using the Leica DM2700 M microscope

combined with an ebq 100-04 mercury lamp (Leica Microsystems Inc.). To record the formation dynamics of liquid residues on the micropillars, a high-speed camera (VEO 710L, Phantom) was combined with the microscope. Two sampling rates, 10^4 and 10^5 fps, were used. The corresponding exposure times were 30 μs and 5 μs, respectively. The model SLR surface (pillar diameter = 30 μm, inter-pillar spacing = 50 μm) was held vertically under the microscope using a home-made XYZ manipulator. The objective focused on the micropillars at the edge of the surface for better visualization. Typically, a liquid drop (~ 3.5 μL) was carefully brought to contact with the micropillars using the home-made XYZ manipulator before it was translated on the microstructured surface along the X axis. The test liquids for high-speed video imaging under microscope include ionic liquid (N^+S^-), Milli-Q water, sodium chloride aqueous solution (26.5 wt%) and mercury.

Liquid residue characterization. The test liquid drop (3.5 μL) was held by a metal ring (inner diameter = 1.2 mm, outer diameter = 2.2 mm) and brought to contact the microstructured surface using a XYZ manipulator. The microstructured surface was then

allowed to translate horizontally at a velocity of 5 mm/min. The resultant liquid residues on the microstructured surface were observed using the microscope operated in the bright field. The diameters of the residual droplets on the micropillared surfaces were measured using ImageJ software, and their volumes were calculated assuming they form spherical caps with contact angles equal to the intrinsic receding angles. The test liquids included ionic liquid (N^+S^-), oleic acid and PDMS. For visualizing the liquid residues on the plant leaves, Neverwet coating and soot-templated superamphiphobic surface, 0.1 mg/mL rhodamine B was added to the test liquid (ionic liquid, N^+S^-). To study the accumulation of solid residues on the model SLR surface, the drop containing 30 wt% colloidal silica was translated back and forth along a linear path on the micropillared surface for 30 cycles (5 mm, 10 cycles/min. Taber Linear Abraser, Taber Industries, USA). The solid residues were observed using the optical microscope under bright field.

Adhesion force measurement. The vertical adhesion forces of the surfaces before and after being polluted by the colloidal silica were measured using a force tensiometer (Krüss, K100). A 3.5 μL water drop was first brought to contact the surface before it was

further compressed for 0.05 mm to have a better liquid-solid contact (compressing velocity = 1 mm/min). Afterwards, the drop was retracted at a speed of 0.5 mm/min until complete departure from the surface. The maximal force during the retraction was regarded as the vertical adhesion force.

Image Analysis. ImageJ and Matlab ® R2018b softwares were used for image analysis. First, the grayscale images were converted into binary ones, from which the liquid-air interfaces were extracted. The liquid-air interfaces in direct contact with the micropillars, typically within 3 μm atop the micropillar surface, were used to determine the local contact angles (fitting the liquid-air interfaces to linear curves gave the slopes, i.e., the tangents of local receding angles). We also measured the inclined angles along the liquid-air interfaces, and the maximal inclined angles were used as the macroscopic contact angles.

Numerical Simulations. Three-dimensional numerical simulations were implemented to study the shape evolution of micro-capillary bridge at the receding contact line on model SLR surfaces. The multiphase flow is simulated using the VOF (volume of fluid) method,

with water and air as the immiscible phases. A model microfluidic device is designed to drive the motion of liquid atop the micropillar array (D = 30 μm, L = 50 μm), see Figure S7. The simulated domain contains ~7.5×10^6 hexahedral cells, and the smallest element size on the micropillar was 0.5 μm. In the simulation, incompressible, Laminar flow model and no-slip boundary condition were adopted. The continuum surface force method was used to include the effect of surface tension, which served as the force source term in the momentum equation (Navier-Stokes equation). The second-order upwind scheme was used to discretize the momentum equation, and the PISO (pressure implicit with splitting of operators) algorithm was used for pressure-velocity coupling. The governing equations (continuity and momentum equations) were solved with ANSYS Fluent software using a pressure-based solver. A typical time step size was 2×10^{-7} s in the simulation. The numerical simulations were performed using Tianhe-2 supercomputer at the National Suprcomputer Centre in Guangzhou (NSCC-GZ).

Supporting Figures

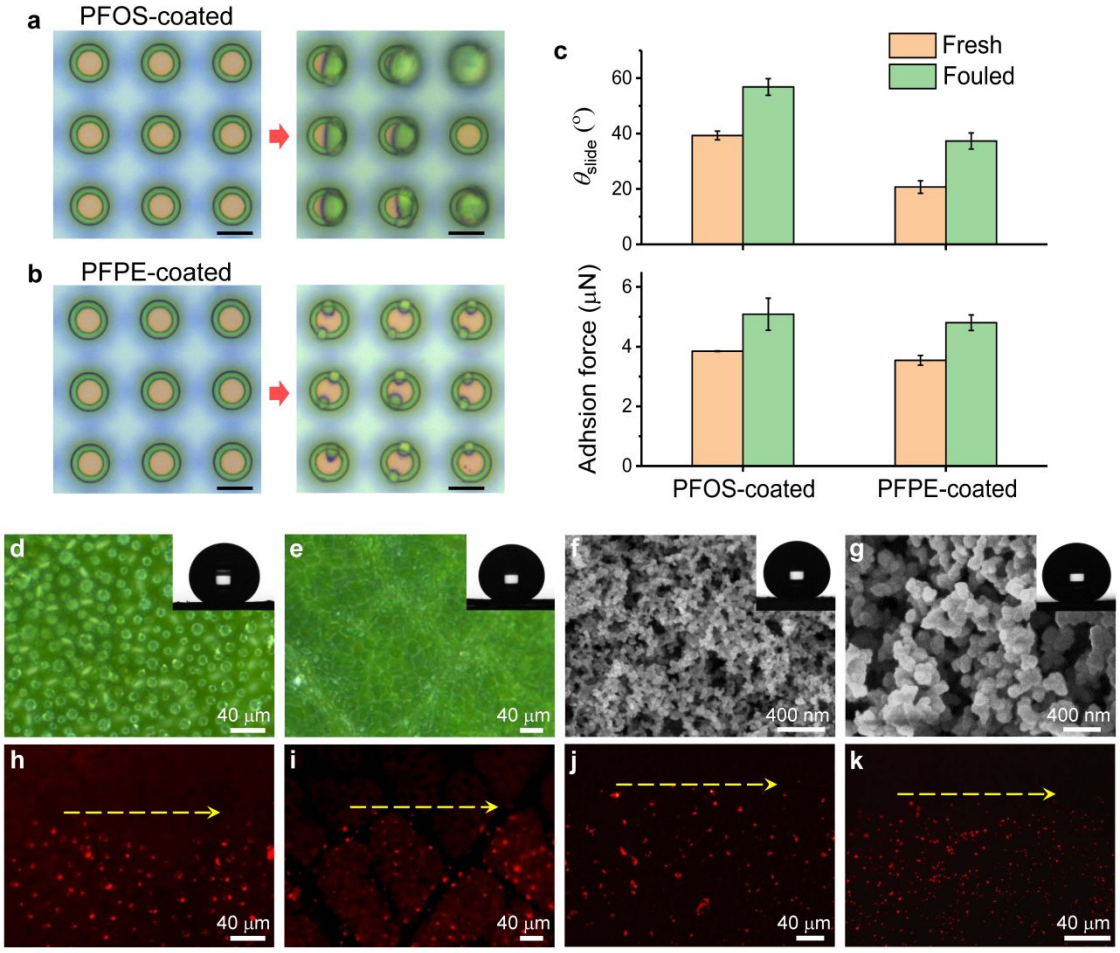

Figure S1. Formation of microscopic liquid residues on various SLR surfaces. (a, b) Microscope images of the micropillared SLR surfaces before and after fouling. The surfaces were coated with PFOS (a) and PFPE (b), respectively. An aqueous drop consisting of 30 wt% colloidal silica was transported on the surfaces along a linear path back and forth for 30 times (5 mm, 10 cycles per minute). Water in the microscopic liquid residues evaporated quickly, leaving the nanoparticles on the micropillars. The scale bars are 10 μm. (c) Sliding angle θ_{slide} and adhesion force on the micropillared surfaces before and after fouling by the nanoparticles. (d, e) Bright-field microscope images of Nelumbo nucifera leaf and Bauhinia blakeana Dunn leaf. (f, g) SEM images of the artificial SLR surfaces, including Neverwet superhydrophobic coating surface (f) and soot-templated superamphiphobic surface (g). The insets show 5-μL test liquid drops on the SLR surfaces. The test liquid is ionic liquid N^+S^- with 0.1 mg/mL rhodamine B. (h, i) Fluorescent microscopic images of the lotus leaf (h) and Bauhinia blakeana Dunn leaf (i), focusing on the same positions as in (d) and (e). (j, k) Fluorescent microscopic images of the Neverwet superhydrophobic coating (j) and soot-templated superamphiphobic surface (k). Bright fluorescent spots were detected on the natural and artificial SLR surfaces, reflecting the formation of microscopic liquid residues. The dash arrows indicate the moving direction of the test drop and also the border of the solid-liquid contact.

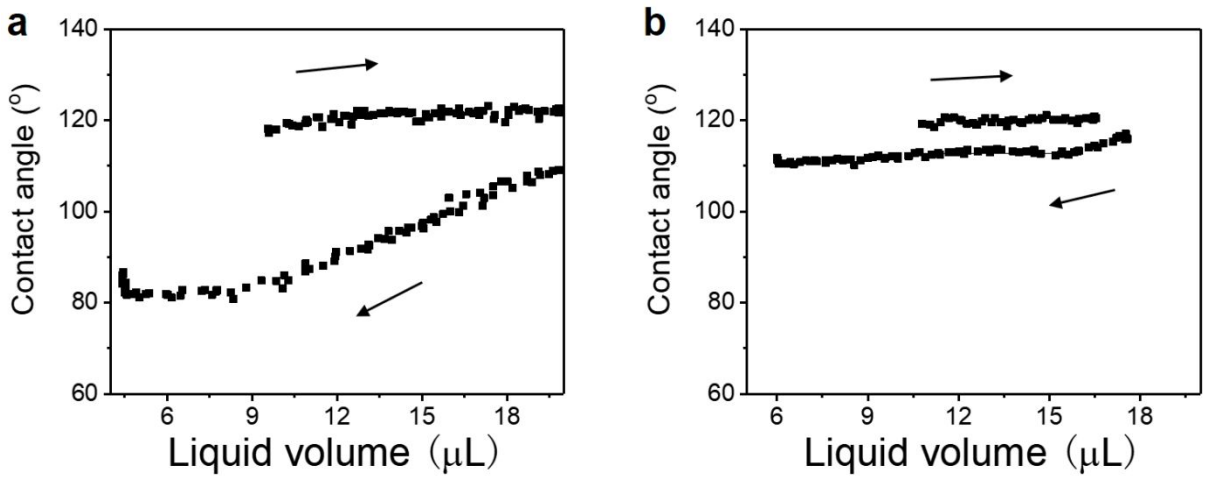

Figure S2. Contact angle hysteresis curves for ionic liquid N^+S^- on PFOS-coated (a) and PFPE-coated (b) surfaces.

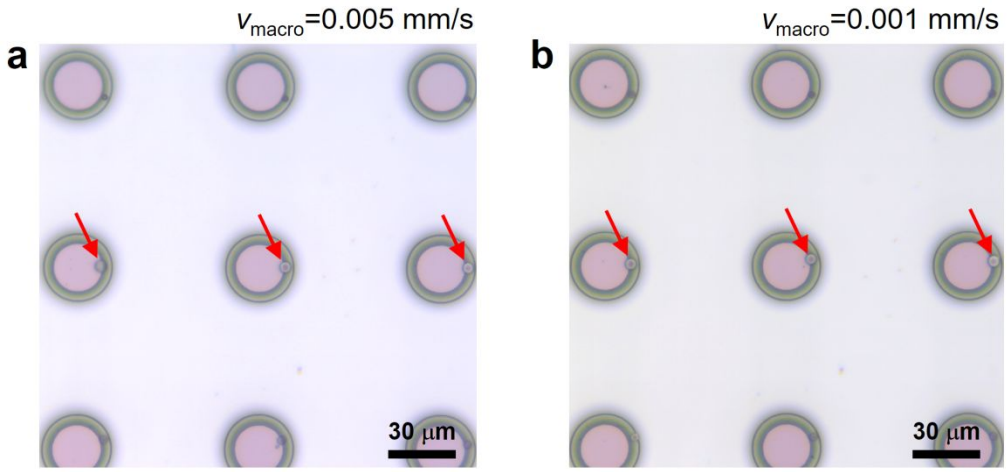

Figure S3. Formation of microscopic liquid residues on PFPE-coated micropillars. The macroscopic drop velocity is 0.005 mm/s (a) and 0.001 mm/s (b), respectively. The moving direction is from left to right.

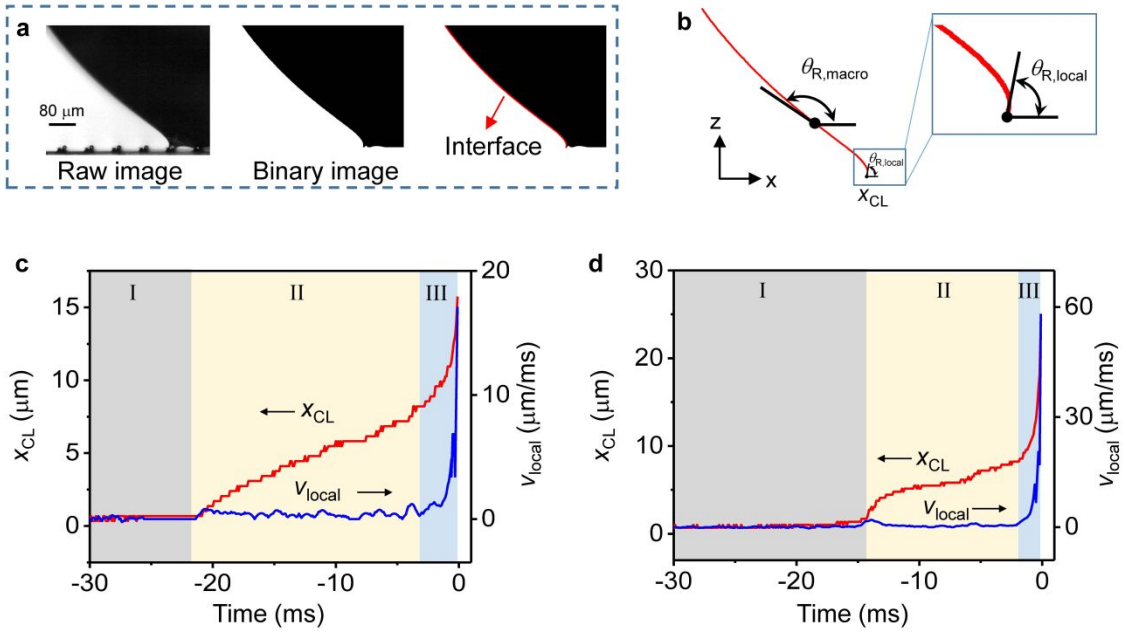

Figure S4. Determination of the position and velocity of three-phase contact line on the micropillar. (a) Method to extract the liquid-air interface from a raw image. The raw image is first transformed to a binary image using ImageJ software. The liquid-air interface is then obtained by detecting the border of the drop using Matlab software. (b) Determination of the contact line position on the micropillar x_{CL}, the local receding angle $\theta_{R,local}$, and the macroscopic receding angle $\theta_{R,macro}$. The local receding angle is measured by fitting a linear line to the liquid-air interface close to the micropillar (typically within 3 μm atop the micropillar). The macroscopic angle is determined by searching the maximal local slope of the liquid-air interface. (c, d) Positions and velocities (v_{local}) of the contact lines on PFOS-coated (c) and PFPE-coated (d) micropillars. The three characteristic stages, i.e., corner pinning (I), slow sliding (II) and accelerated receding (III) stages, are indicated by different background colors.

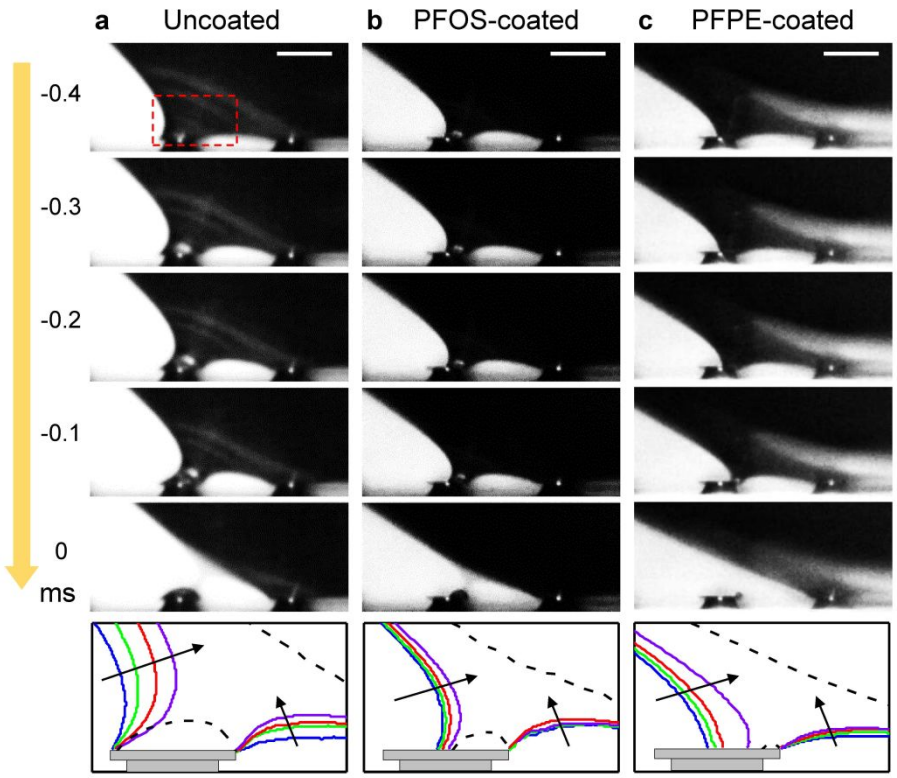

Figure S5. Evolution of micro-capillary bridges on micropillars with different surface coatings before pinch-off. The micropillars are uncoated (a), PFOS-coated (b) and PFPE-coated (c). The liquid-air interfaces in the dashed red box at -0.4 ms (solid blue lines), -0.3 ms (solid green lines), -0.2 ms (solid red lines), -0.1 ms (solid purple lines), and 0 ms (dashed black lines) are given below the microscopic images. Time 0 represents the moment when the micro-capillary bridge ruptures. The macroscopic moving speed of the test drop is ~0.1 mm/s. The test liquid is ionic liquid (N^+S^-). Scale bars, 40 μm.

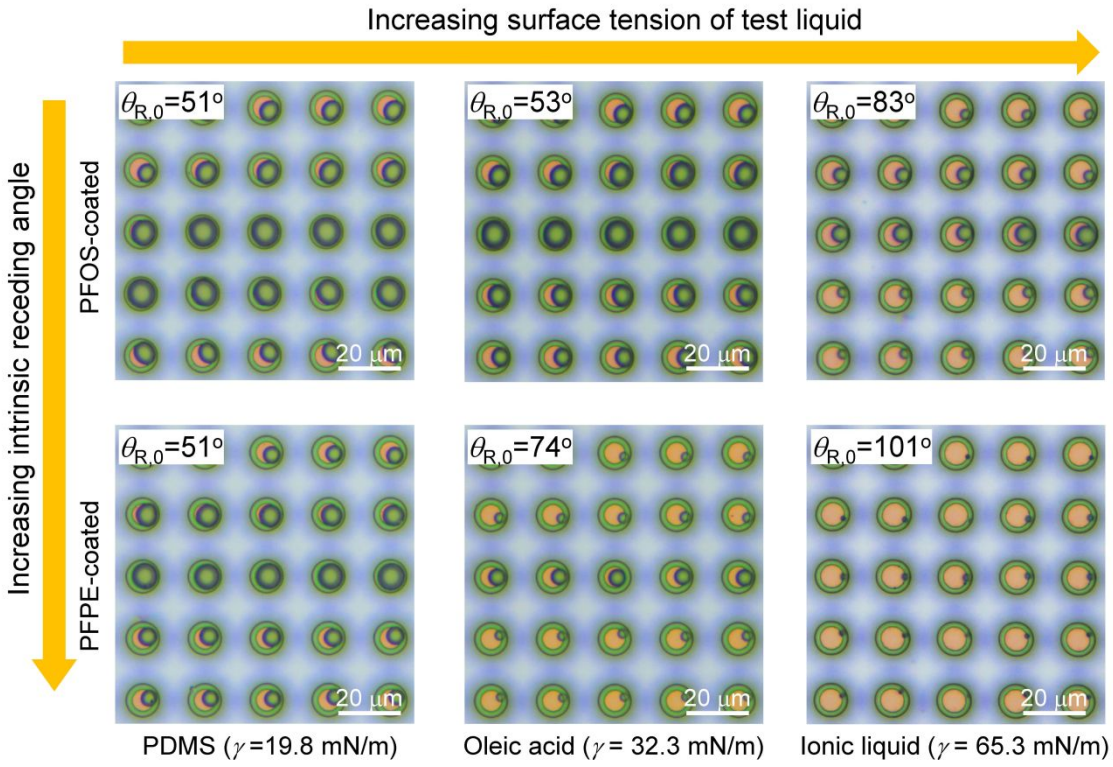

Figure S6. Microscopic images showing the liquid resides on the micropillars. By increasing the intrinsic receding angle (using PFPE instead of PFOS as the coating material), and using test liquids with larger surface tension, the size of liquid residues on the model SLR surface becomes smaller. Macroscopic drop velocity is ~ 0.1 mm/s.

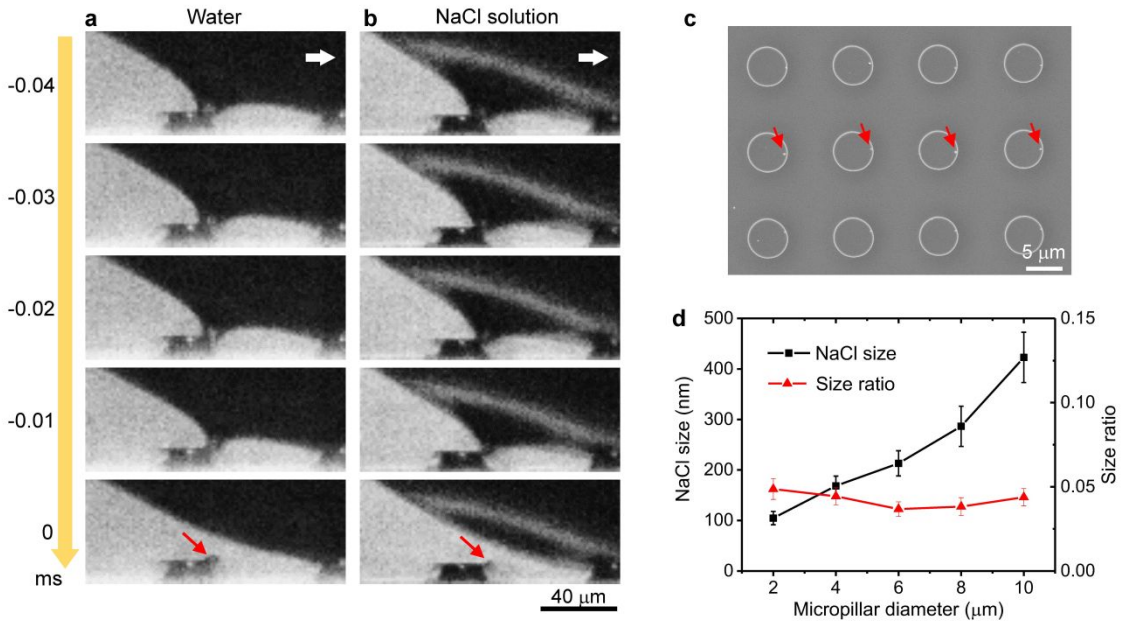

Figure S7. Formation of microscopic liquid residues on PFPE-coated SLR surfaces. (a, b) Dynamics of micro-capillary bridge before pinch-off for water ($\gamma \sim 72.3 \pm 0.2$mN/m) and saturated sodium chloride (NaCl) solution (26.5 wt%, $\gamma = 82.4 \pm 0.2$ mN/m). The scale bar is 40 μm. Macroscopic drop velocity is ~ 0.1 mm/s. The residue water droplet disappears within 0.2 s due to evaporation. For saturated NaCl solution, as water evaporates, the solute NaCl is left on the micropillars. (c) SEM image of micropillared SLR surface with NaCl residues. Four NaCl residues are indicated by the red arrows. (d) The size of NaCl residue as a function of micropillar diameter (inter-pillar spacing = pillar diameter). The size of liquid residues decreases with the pillar diameter. However, the size ratio of the residue to the micropillar does not decrease when the micropillar size decreases, implying that decreasing micropillar size cannot eliminate liquid residues.

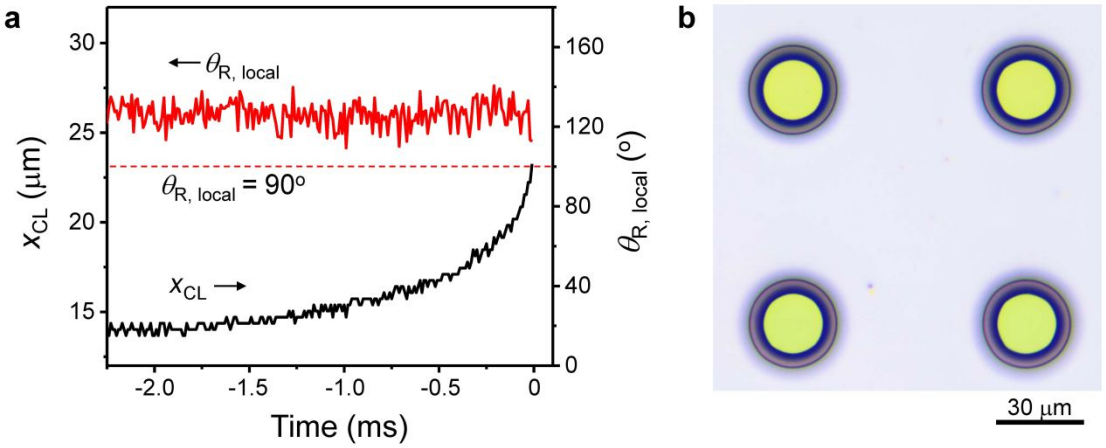

Figure S8. No liquid residues observed when a mercury drop slides on micropillared surface. (a) Position (x_{CL}) of contact line and local receding contact angle ($\theta_{R,local}$) of mercury on the uncoated micropillar. (b) Microscopic image showing that the micropillars are free of mercury residues. Macroscopic drop velocity is ~0.1 mm/s.

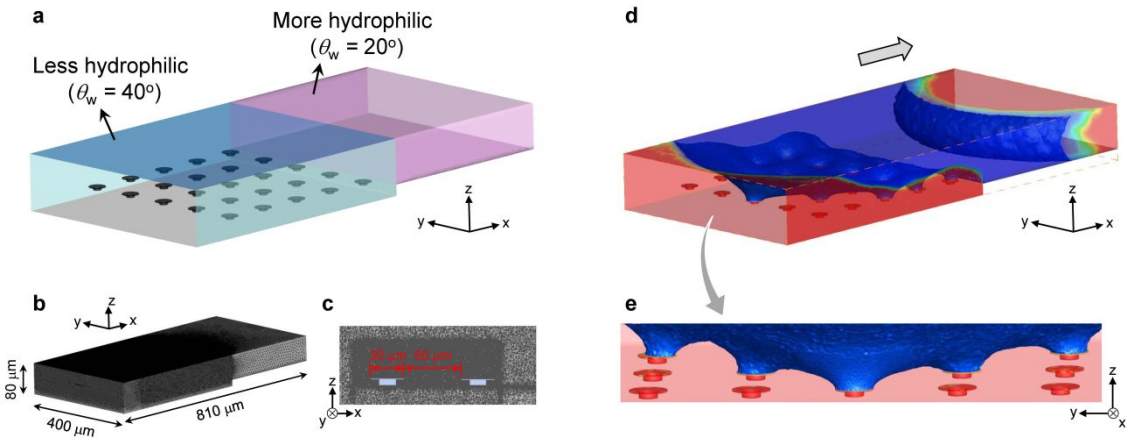

Figure S9. Simulation details of receding contact line on a micropillared surface. (a) The geometry of microfluidic chamber and the wall boundary conditions used in the simulation. The walls on the right have a smaller water contact angle (more hydrophilic) than that on the left, enabling water to migrate from left to right. (b) The meshed microfluidic chamber and its characteristic sizes. (c) The diameter of the micropillar and the inter-pillar spacing. A finer mesh size is used around the interest micropillars to have a higher spatial resolution. (d) Water in the microfluidic chamber migrates spontaneously to the more hydrophilic region (along x direction). (e) The micro-capillary bridges can be observed at the receding tail.

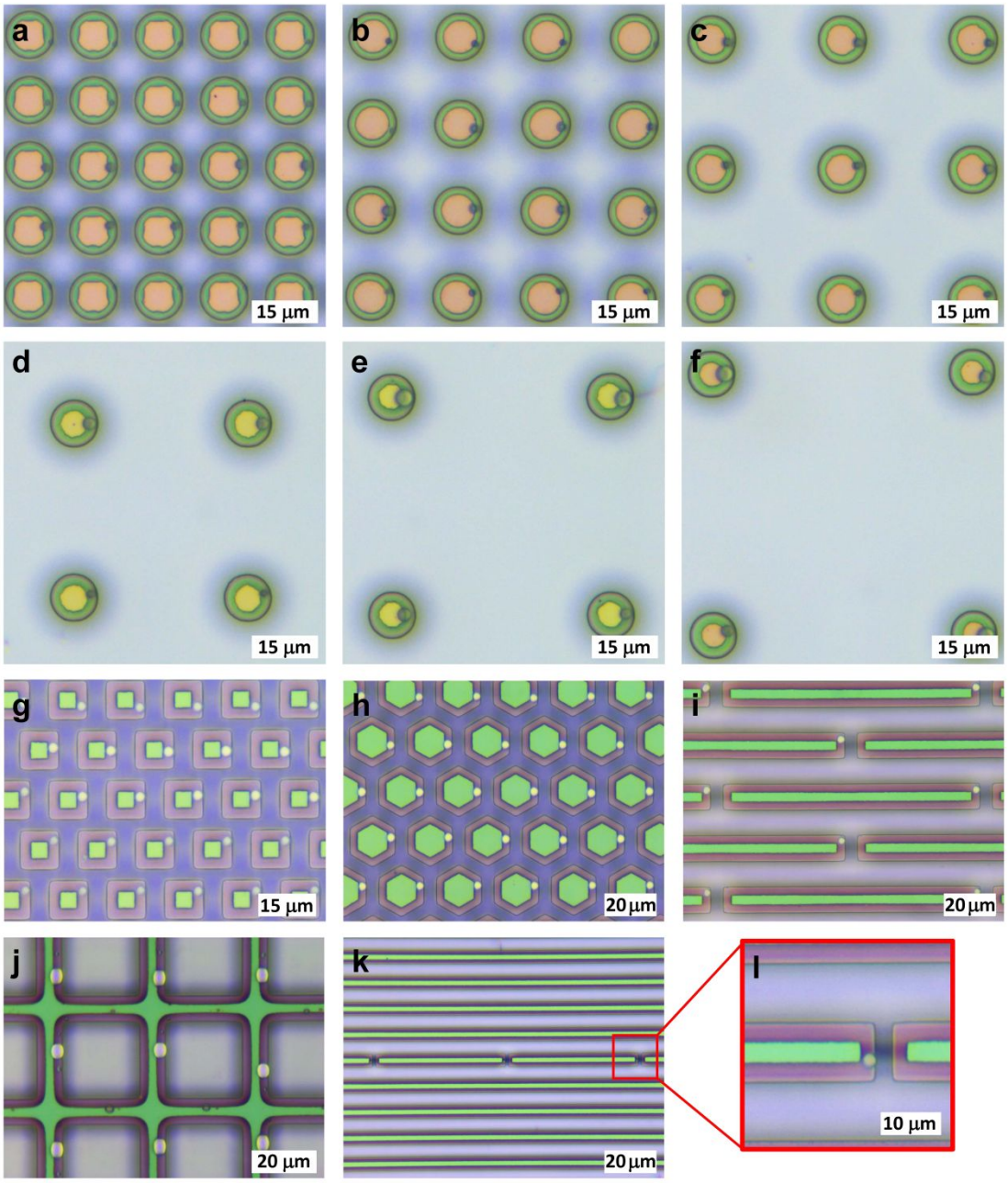

Figure S10. Formation of microscopic liquid residues on PFPE-coated SLR surfaces with different microstructures. (a-f) Influence of inter-pillar spacing on the formation of microscopic liquid residues. It can be observed that microscopic liquid residues were formed on all micropillared SLR surfaces. The size of the liquid residues on the micropillars increased with increasing inter-pillar spacing. (g-l) Influence of the geometry of microstructure on the formation of liquid residues. It can be observed that liquid residues always form when the contact line recedes across the discrete microstructures. All the surfaces are coated with PFPE. The test liquid is ionic liquid (N^+S^-). The drop was transported on the surface from left to right at a velocity of ~0.1 mm/s.

Supporting Tables

Table S1. Contact angles, fitting parameters and governing dimensionless numbers for ionic liquid (N^+S^-) on the model SLR surfaces.

Surface coating	Contact angles[a] [°]		Fitting parameters		Dimensionless numbers[c]			
	$\theta_{R,0}/\theta_{A,0}$	$\theta_{R,m}/\theta_{A,m}$	$\theta_{R,0}$	$\ln(C\gamma/\gamma_w)$	*Ca*	*Bo*	*We*	*Oh*
Uncoated	52/68	125/172	N/A[b]	N/A	6×10^{-4}—N/A[d]	4×10^{-5}	3×10^{-9}—N/A	11.2
PFOS-coated	83/111	137/171	77 ± 4	1.4 ± 0.4	6×10^{-4}—0.2	4×10^{-5}	3×10^{-9}—3×10^{-4}	11.2
PFPE-coated	101/110	155/175	106 ± 5	0.7 ± 0.2	6×10^{-4}—0.9	4×10^{-5}	3×10^{-9}—6×10^{-3}	11.2

[a] $\theta_{R,0}$ and $\theta_{A,0}$ are the intrinsic receding and advancing contact angles measured on flat surfaces with the same surface coating. $\theta_{R,m}$ and $\theta_{A,m}$ are macroscopic receding and advancing contact angles meausred on the model SRL surfaces using a goniometer.

[b] Receding of the contact line on the uncoated micropillar is hardly observed, therefore fitting to Cox-Voinov relation ($\theta_{R,local}^3 = \theta_{R,0}^3 - 9\ln(C\gamma/\gamma_W)Ca$) is not feasible.

[c] Capillary number: $Ca = \eta v/\gamma$, Bond number: $Bo = g\rho R^2/\gamma$, Weber number: $We = gv^2R/\gamma$. For ionic liquid N^+S^-, the following values are used for calculation: viscosity η = 0.4 Pa·s, surface tension γ = 65.3 mN/m, density ρ =1300 kg/m^3, characteristic size of the micro-capillary bridge R = 15 μm, and gravitational acceleration g = 9.8 m/s^2. The macroscopic moving speed of the drop (~0.1 mm/s), and the highest detectable receding velocities of the contact lines on the micropillars (~30 mm/s and 140 mm/s for PFOS-coated and PFPE-coated micropillars, respectively), are used to determine the range of *Ca* and *We*.

[d] Maximal receding velocity of the contact line on the uncoated micropillar is not accessible, as explained above.

Table S2. Physical properties of the test liquids and their contact angles on the model SLR surfaces. The physical properties include surface tensions (γ), viscosities (η) and densities (ρ) of the test liquids. The contact angles include the intrinsic contact angles ($\theta_{R,0}$) and the local receding contact angles ($\theta_{R,local}$ (t→0)) just before pinch-off of the micro-capillary bridges.

Liquid[a]	γ [b] (mN/m)	η [c] (Pa·s)	ρ [d] (g/cm^3)	$\theta_{R,0}$ (°) [e]			$\theta_{R,local}$ (t→0) (°) [f]		
				Un-coated	PFOS-coated	PFPE-coated	Un-coated	PFOS-coated	PFPE-coated
N^+S^-	65.3	0.40	1.3	52 ± 2	83 ± 2	101 ± 2	25 ± 3	43 ± 7	78 ± 11
H_2O	72.3	0.0009	1.0	57 ± 1	83 ± 2	112 ± 2	20 ± 5	40 ± 7	85 ± 3
NaCl	82.4	0.0014	1.2	67 ± 1	96 ± 2	118 ± 1	37 ± 6	61 ± 14	71 ±13
Hg	~ 480	0.0015	13.5	133 ± 1	114 ± 5	147 ± 1	127±5	96/81±8[g]	134 ±9

[a] NaCl: sodium chloride aqueous solution, 26.5 wt%; Hg: mercury.

[b] Surface tensions of N^+S^-, H_2O and NaCl solution are measured using pendant drop method at 25 °C. Surface tension of Hg is from literature (Trans. Faraday Soc., 1946, 42, 526).

[c] Viscosity of N^+S^- is measured using falling ball method. Viscosities of H_2O, NaCl solution and Hg are extracted from literature (J. Phys. Chem. Ref. Data 1981, 10, 71-88; 2012, 41, 033101).

[d] Densities of N^+S^-, H_2O and NaCl solution are determined by a standard method, i.e., dividing their weights by their volumes. Density of Hg is from literature (J. Phys. Chem. Ref. Data 2012, 41, 033101).

[e] Intrinsic receding angles are measured using a conventional goniometer.

[f] The local receding angles of the test liquids just before detaching from the micropillars are determined through high-speed video imaging under microscope at a sampling speed of 10^5 frames per second (0.01 ms time resolution).

g) The PFOS coating in contact with mercury is not stable. In a set of experiments, we observed $\theta_{R,local} > 90^o$, while in another set of experiments, we observed $\theta_{R,local} < 90^o$.

Supporting Movies

Movie S1. Stepwise pinning-depinning processes of the receding contact line on the micropillared SLR surfaces with different coatings.

Movie S2. Evolution dynamics (time resolution: 10^{-4} s) of micro-capillary bridges on SLR surfaces with different coatings.

Movie S3. High-speed evolution dynamics (time resolution: 10^{-5} s) of micro-capillary bridges on SLR surfaces with different coatings, showing the detailed necking and pinch-off processes occurring in the last 0.1 ms.

Movie S4. High-speed evolution dynamics (time resolution: 10^{-5} s) of micro-capillary bridge for a metal liquid (Hg) drop on the micropillar, showing neither necking nor pinch-off of the micro-capillary bridge.